Magnetoabsorption and spin polarization inversion in GaAs/AlGaAs quantum wells

G. M. Jacobsen,[1] V. Lopes-Oliveira,[2] V. Laurindo, Jr.,[1] A. Malachias,[3] B. D. Moreno,[4] Yu. I. Mazur,[5] G. J. Salamo,[5] G. E. Marques,[1] E. Marega, Jr.,[6] V. Lopez-Richard,[1,*] and M. D. Teodoro[1,†]

[1]*Departamento de Física, Universidade Federal de São Carlos, 13565-905 São Carlos, SP, Brazil*

[2]*Departamento de Física, Universidade Estadual de Mato Grosso do Sul, Dourados, 79804-970 Mato Grosso do Sul, Brazil*

[3]*Departamento de Física, Universidade Federal de Minas Gerais, 30123-970 Belo Horizonte, MG, Brazil*

[4]*Canadian Light Source Inc., 44 Innovation Boulevard, Saskatoon, S7N 2V3 Saskatchewan, Canada*

[5]*Institute for Nanoscience and Engineering, University of Arkansas, Fayetteville, Arkansas 72701, USA*

[6]*Instituto de Física de São Carlos, Universidade de São Paulo, 13566-590 São Carlos, SP, Brazil*

(Received 23 April 2024; accepted 28 June 2024; published 11 July 2024)

The impact of the growth orientation on spin dynamics in GaAs/AlGaAs quantum wells (QWs) is explored through magnetophotoluminescence measurements. Samples grown on both (100) and (311)A GaAs surfaces exhibit intensity oscillations at high magnetic fields, characteristic of magnetoabsorption arising from interband transitions between Landau levels when excited near resonance. Notably, the (311)A surface reveals optical responses rarely observed on the conventional (100) surface, including an inversion in circular polarization degree influenced by both excitation power and temperature. To elucidate these findings, we develop an eight-level model encompassing electron and hole excited states. Our analysis demonstrates that thermalization is the primary and sufficient factor responsible for reproducing spin inversion with external parameters.

DOI: 10.1103/PhysRevB.110.035417

I. INTRODUCTION

Spin manipulation in semiconductors has garnered attention in recent years, driven by the growing interest in spintronics and quantum information. The precise control of spins is essential for the advancement of these applications, emphasizing the pivotal role of semiconductor materials in facilitating breakthroughs in spin-related technologies [1–3]. Numerous studies have demonstrated the manipulation of spin through external parameters, including electric field [4,5], excitation power [6,7], and thermal annealing [8]. Spectroscopic techniques, such as magnetophotoluminescence (MPL), offer a means to analyze the predominant spin character. It enables the determination of Zeeman splitting and the degree of circular polarization (DCP), providing insights into the spin properties and dynamics under investigation [9,10].

The influence of lattice mismatching on spin and the corresponding electronic structure can vary significantly depending on the semiconductor structure. In bulk materials, strain induced by lattice mismatch leads to a reduction in crystal symmetry, thereby breaking certain degeneracies [11,12]. Quantum heterostructures, including quantum dots [13], nanowires [14,15], and quantum wells (QWs) [16,17], exhibit alterations in their electronic and optical characteristics under strain. While traditionally grown on [100]-oriented substrates, past research suggests that high-index substrates may offer superior optical qualities [18,19], potentially serving as viable alternatives for spin-photon interfaces. For instance, whereas strain's impact on GaAs/AlGaAs heterostructures grown on (100)-oriented GaAs substrates is minimal (typically below 1%), high-index orientations introduce complexities in the valence band structure and result, for example, in reduced effective masses [20,21]. These factors could substantially modify the optical, electronic, and spin properties of such structures.

In this study, we investigate the impact of magnetoabsorption on exciton spin relaxation in a GaAs/AlGaAs quantum well (QW) system grown on both (100) and (311)A GaAs substrates. We observe marked oscillations in the integrated photoluminescence intensity at high magnetic fields, particularly when the excitation energy closely matches the resonance of the quantum well emission, attributed to interband transitions originating from Landau levels (LLs). Notably, on the (311)A QW surface, we observe a reversal in the degree of circular polarization under the influence of a magnetic field, with this effect becoming more pronounced with increased excitation power and/or temperature. We interpret this phenomenon as evidence of a thermalization process taking place within the system, prompting us to propose alternative explanations compared to the existing assumptions found in the literature [22]. This new perspective sheds light on the underlying mechanisms driving the observed changes in the DCP under the influence of a magnetic field, offering fresh insights into the dynamics of exciton spin relaxation in our GaAs/AlGaAs QW system.

II. METHODS

Two multiquantum well samples of GaAs/$Al_{0.36}Ga_{0.64}As$ (5.5 nm well), and GaAs/$Al_{0.33}Ga_{0.67}As$ (5.2 nm well) were simultaneously grown by molecular beam epitaxy on (100) and (311)A GaAs surfaces, respectively. Magnetophotoluminescence measurements in Faraday geometry from 3.6 to

*Contact author: vlopez@df.ufscar.br
†Contact author: mdaldin@gmail.com

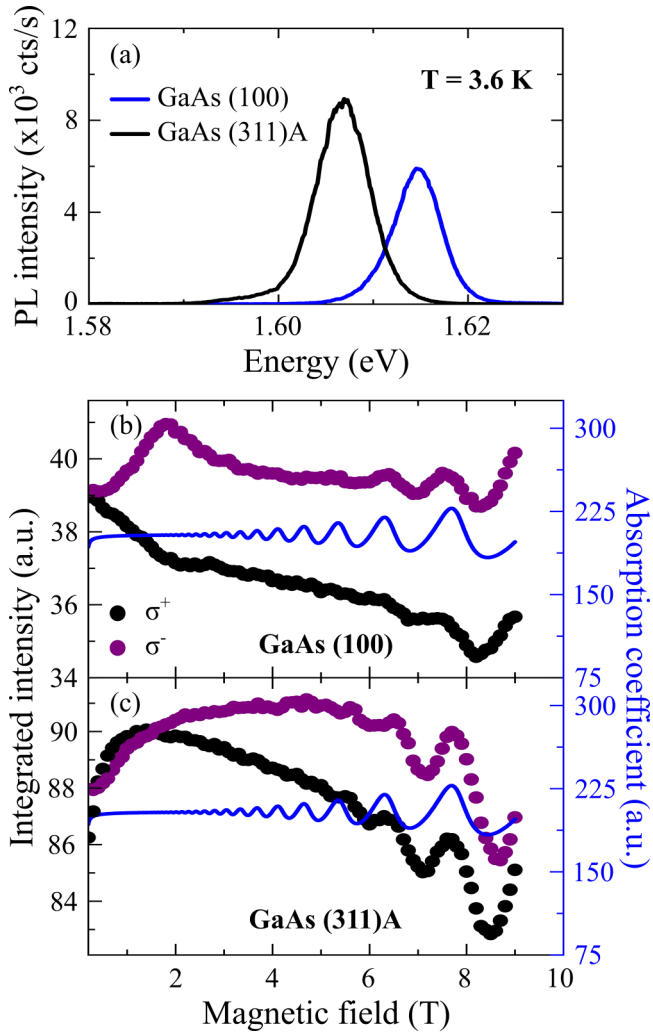

FIG. 1. (a) Photoluminescence spectra of the GaAs/AlGaAs QWs grown in different substrate orientations: GaAs (100) (blue) and GaAs (311)A (black), respectively. The excitation power is 0.5 μW and the temperature is 3.6 K. Integrated PL intensity and calculated magnetoabsorption coefficient of the GaAs QW vs magnetic field for samples grown on (b) (100) and (c) (311)A GaAs substrates. The origin of the shoulder at 2 T for the σ^- integrated intensity for the (100) sample is presented in Ref. [28].

60 K were performed using a helium-closed cycle cryostat (Attocube/Attodry 1000). The samples were optically investigated by means of a confocal microscope setup, with an excitation laser energy at 1.698 eV (PicoQuant-LDH-730) with a constant power of 0.5 μW (unless otherwise stated) focused on a spot diameter of 1 μm. A set of polarizers were used to excite the samples in linear basis and turn the emitted luminescence in σ^+ and σ^- circular components, which were dispersed by a 75 cm spectrometer and detected by a silicon CCD (Andor/Shamrock-Idus).

III. RESULTS AND DISCUSSION

The photoluminescence spectra of the examined structures, obtained at a temperature of 3.6 K, are illustrated in Fig. 1(a). The emissions from the quantum wells are notably centered at 1.615 eV (with a full width at half maximum of 5.2 meV) for the GaAs (100) substrate orientation, and at 1.608 eV (with a full width at half maximum of 5.6 meV) for the GaAs (311)A substrate orientation [23]. The shift between the PL spectra of the QWs results from the generation of piezoelectric fields, effective mass anisotropy, and the interface roughness due to the density of the growth steps for the (311)A surface [24–27].

The integrated intensity of each photoluminescence (PL) emission, plotted against the applied magnetic field for both samples, is depicted in Figs. 1(b) and 1(c). As the applied magnetic field increases, there is a discernible splitting of the two circular emission components, accompanied by pronounced oscillations at higher magnetic fields. These oscillations are interpreted as arising from interband transitions between Landau levels. Under an applied external magnetic field along the sample growth direction (z), electrons and holes experience the Landau quantization of the oscillatory motion in the x-y plane [29,30]. When the energy ($\hbar\omega$) of the excitation photon matches the energy of a LL subband, a maximum of absorption is expected. Hence, exciting close to the QW emission is vital to observe such a behavior (see Fig. S1 from the Supplemental Material [31] where no oscillations are found for a higher energy excitation), otherwise this resonant effect becomes damped by additional interference of scattering and relaxation mechanisms. In the right axis of Figs. 1(b) and 1(c) we present the result of a model based on the magnetoabsorption, where the carrier photogeneration α can be calculated as [32]

$$\alpha(\hbar\omega, B) \propto \frac{|ep_{cv}^{\pm}|^2 B}{\hbar\omega} \times \sum_N \frac{\sqrt{\sqrt{F^{\pm}(N,B)^2+\delta^2}+F^{\pm}(N,B)}}{\sqrt{F^{\pm}(N,B)^2+\delta^2}}, \quad (1)$$

where $|ep_{cv}^{\pm}|$ is the optical transition matrix element, $\delta = 3.5$ meV is a lifetime energy broadening, and $F^{\pm}(N,B) = \hbar\omega - (E_c^{\pm}(N,B) - E_v^{\pm}(N,B))$, where $E_c^{\pm}(N,B) - E_v^{\pm}(N,B)$ is the energy difference between LLs indexed by N in the conduction and valence bands with a given spin, under an applied magnetic field. In order to calculate the conduction and valence band energies for both samples, we used the in-plane hole effective mass, electron, and hole g-factor parameters as $m_h^* = 0.11m_0$, $g_e = 0.44$, and $g_h = -2.6$, respectively [33]. Moreover, we extracted an electron effective mass of $m_e^* = 0.077m_0$ and $0.071m_0$ for the growth GaAs-surfaces (100) and (311)A, respectively.

The panels in Fig. 2 illustrate the variation of the degree of circular polarization with respect to the magnetic field in the Faraday geometry for both samples. The DCP is defined as the difference between the integrated intensities of the σ^+ and σ^- spin components divided by their sum, expressed as $DCP = \frac{I_{\sigma^+} - I_{\sigma^-}}{I_{\sigma^+} + I_{\sigma^-}}$. Here, $I_{\sigma^\pm}$ represents the integrated intensity of the corresponding PL spectrum for each spin component. Figure 2(a) showcases the variation of the DCP for the (100) sample at a temperature of 3.6 K, under various excitation laser powers. Notably, the polarization degree exhibits negative values, peaking at an absolute maximum around 1.8 T. This distinct feature emerging around 1.8 T has been recently elucidated as a consequence of the interplay between

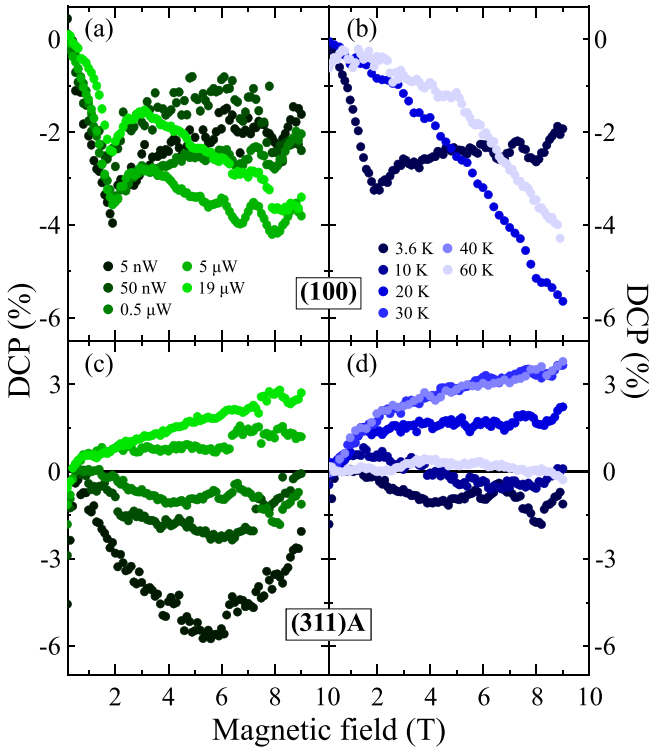

FIG. 2. Magnetic field dependence of the degree of circular polarization measured for various values of incident laser power (left panels) and temperature (right panels) for the samples grown on GaAs substrates oriented along the (100) [(a) and (b)] and (311)A [(c) and (d)] surfaces. The temperature for the excitation power dependence was kept constant at 3.6 K while the excitation power for the temperature ramp was set at 0.5 μW.

short-range interactions and spin-flip scattering, a modulation governed by the momentum relaxation time as discussed in Ref. [28]. Moreover, at high magnetic fields and under intense excitation powers, discernible oscillations are observable. It's noteworthy that the overall magnetic behavior remains consistent even with an increase in laser power. In contrast, as the temperature rises, the DCP exhibits an almost linear increase, as depicted in Fig. 2(b). The temperature increment results in the suppression of both the shoulder around 1.8 T and the oscillatory behavior observed at high magnetic fields, indicative of a breakdown in coherence. As the temperature elevates, such as at 60 K, the DCP diminishes until reaching a fully depolarized state at 100 K (not illustrated here).

To contrast optical and spin memory, the DCP was examined in a GaAs/AlGaAs (311)A multi-QW under the same conditions as the (100) sample and depicted in Figs. 2(c) and 2(d). Surprisingly, in this scenario, the DCP exhibits a strong dependence on the excitation power, as illustrated in Fig. 2(c). It reaches a depolarized state near 0.5 μW and displays a monotonic inversion as the laser power increases. At a constant excitation power of 0.5 μW and various temperatures [Fig. 2(d)], a temperature rise (approximately around 10 K) results in an unpolarized state, followed by a monotonic inversion of the DCP's sign at higher temperatures. Eventually, at 60 K, saturation occurs, leading to depolarization.

According to Figs. 1(b) and 1(c), the intensity of the emitted light follows the magnetic field quantization of the bulk energy states where the main photogeneration of electrons and holes takes place. The correlation of the absorption quantization and the PL emission indicates that the magnetic field quantization of the excited states and the amount of photogenerated carriers during resonant absorption impacts the thermalization taking place at the conduction and valence band ground states. This introduces additional, yet relevant, ingredients to the whole spin dynamics that can produce an inversion of the spin polarization with incoming power and temperature as illustrated in Figs. 2(c) and 2(d), respectively.

Let's first note that the polarization inversion by increasing incident power and temperature has already been reported. In Ref. [22], the authors describe the PL polarization behavior in type-II InSb/InAs nanostructures. At low excitation rates and temperatures below 10 K, where only ground electron and hole states are populated, they observe nearly 100% PL polarization. This high polarization is explained by the total spin alignment of electrons in the InAs conduction band and heavy holes in the InSb layer, attributed to the Zeeman effect and selection rules for optical transitions. As temperature or excitation power density increases, causing the population of higher-energy states, there is an anticipated decrease in the observed polarization degree. Intriguingly, however, an inversion of polarization eventually occurs. The authors noted that this observed polarization inversion cannot be straightforwardly explained by a simple thermal population model. To reconcile experimental data and theory, they put forward a conjecture involving contrasting recombination efficiencies for optical transitions with distinct spin sublevels. They argue that in the studied type-II system, where the oscillator strength is affected by the spatial separation of electron and hole wave functions and the potential profile near the interface, modulated by temperature and excitation rate, could play a role. Furthermore, the authors suggest that the recombination and spin dynamics of "bright" and "dark" excitons could contribute to the observed phenomena. However, they clarify that the paper does not delve into an accurate treatment of these aspects. Instead, they employ phenomenological parameters to describe the relative recombination efficiency of optical transitions involving electrons with spin "up" and spin "down."

However, we can now unequivocally demonstrate that the effect they observed can extend even to more traditional materials, such as GaAs/AlGaAs systems, where no band inversion is anticipated, confirming that thermalization is indeed the predominant factor. Therefore, there is no necessity to hypothesize a spin imbalance in the recombination efficiency to explain the polarization inversion observed with either temperature or power. The factors necessary for these effects are adequately elucidated in the subsequent discussion.

The most basic model we can formulate to account for the full effects here described has been represented in Fig. 3(a): two Zeeman spin-split excited states within each band, with energies $E_{ex}^{\uparrow\downarrow}$ and $E_{hx}^{\uparrow\downarrow}$ for electrons and holes, respectively, and the respective spin-split ground states, $E_{e0}^{\uparrow\downarrow}$ and $E_{h0}^{\uparrow\downarrow}$, from

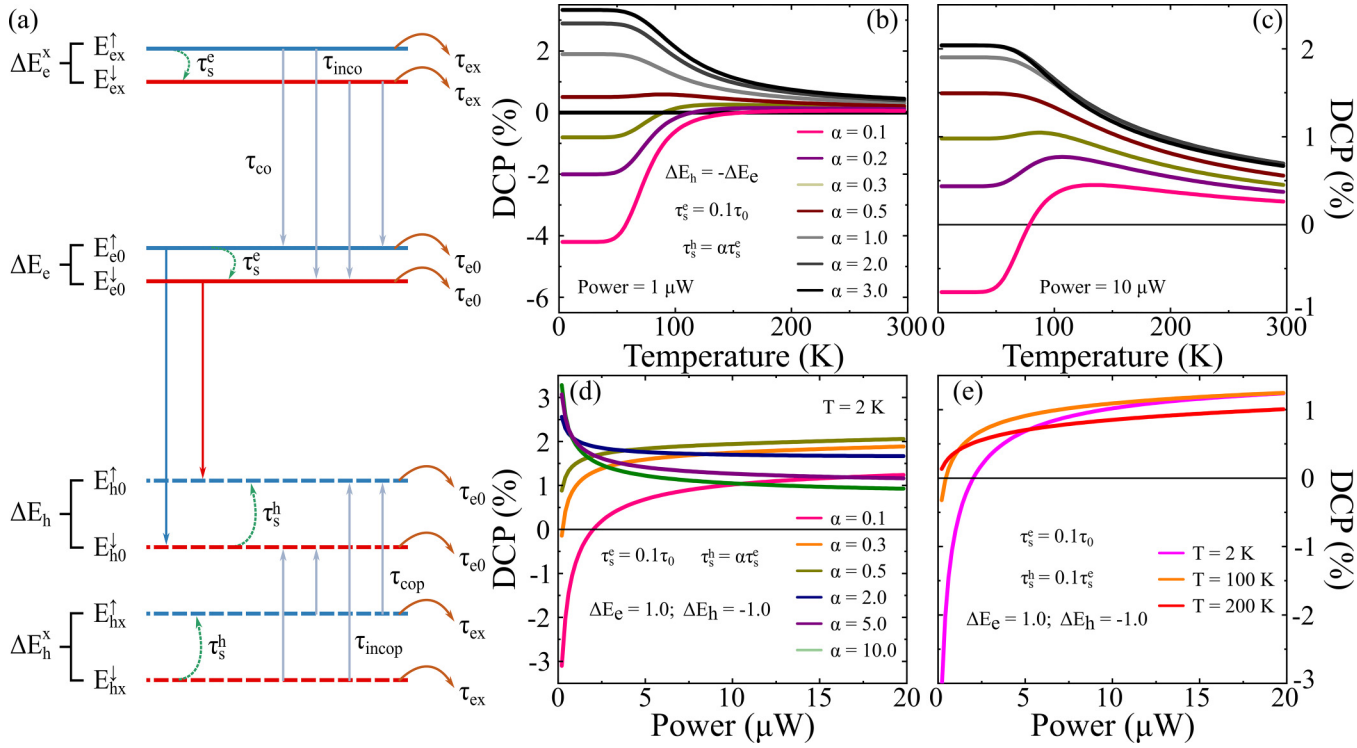

FIG. 3. (a) Eight-level system diagram, being the four upper levels the conduction band ($E^{\uparrow}_{e0}$ and $E^{\downarrow}_{e0}$ corresponding to ground states, $E^{\uparrow}_{ex}$ and $E^{\downarrow}_{ex}$ corresponding to excited levels) and the four lower levels the valence band ($E^{\uparrow}_{h0}$ and $E^{\downarrow}_{h0}$ corresponding to ground states, $E^{\uparrow}_{hx}$ and $E^{\downarrow}_{hx}$ corresponding to excited levels), indicating optical recombination times and energy levels variation. DCP vs temperature for α values from 0.1 to 3.0 for excitation powers equals to (b) 1 μW and (c) 10 μW. Both for $\tau^e_s = 0.1\tau_0$, $\tau^h_s = \alpha\tau^e_s$, and $\Delta E_h = -\Delta E_e$. DCP vs excitation power for (d) α values from 0.1 to 10.0 and $T = 2$ K, and (e) $\alpha = 0.1$ and different values of T. Both for $\tau^e_s = 0.1\tau_0$, $\tau^h_s = \alpha\tau^e_s$, $\Delta E_e = 1.0$ meV and $\Delta E_h = -1.0$ meV.

which the optical recombination takes place at a rate $1/\tau_0$ (independently on spin).

Each pair of Zeeman split states in the conduction (valence) band may undergo spin flips at rates $1/\tau_s^{e(h)}$. In turn, the energy relaxation between excited and ground states may take place through spin-coherent processes characterized by $1/\tau_{\rm co}$ or incoherent spin-flip transitions $1/\tau_{\rm inco}$. The DCP oscillations measured at high fields are unequivocal proofs of the presence of coherent relaxation channels. Thus, the spin dynamics and electron-hole pair recombination can be emulated by solving the following set of stationary equations introducing a CW pumping rate, R, with four equations for each band (conduction and valence, respectively):

$$\frac{dn^{\uparrow}_{ex}}{dt} = R - n^{\uparrow}_x\left(\frac{1}{\tau_{\rm co}} + \frac{1}{\tau_{\rm inco}}\right) - \frac{n^{\uparrow}_x}{\tau^e_s} f\left(\Delta E^x_e, t\right) + \frac{n^{\downarrow}_x}{\tau^e_s} f\left(-\Delta E^x_e, t\right) - \frac{n^{\uparrow}_x}{\tau^{ex}} = 0, \tag{2}$$

$$\frac{dn^{\downarrow}_{ex}}{dt} = R - n^{\downarrow}_x\left(\frac{1}{\tau_{\rm co}} + \frac{1}{\tau_{\rm inco}}\right) - \frac{n^{\downarrow}_x}{\tau^e_s} f\left(-\Delta E^x_e, t\right) + \frac{n^{\uparrow}_x}{\tau^e_s} f\left(\Delta E^x_e, t\right) - \frac{n^{\uparrow}_x}{\tau^{ex}} = 0, \tag{3}$$

$$\frac{dn^{\uparrow}_{e0}}{dt} = n^{\uparrow}_x\tau_{\rm co} + \frac{n^{\downarrow}_x}{\tau_{\rm inco}} - \frac{n^{\uparrow}_0}{\tau^e_s} f(\Delta E_e, t) + \frac{n^{\downarrow}_0}{\tau^e_s} f(-\Delta E_e, t) - \frac{n^{\uparrow}_0}{\tau_{e0}} - \frac{n^{\uparrow}_0 p^{\uparrow}_0}{\tau_0} = 0, \tag{4}$$

$$\frac{dn^{\downarrow}_{e0}}{dt} = n^{\downarrow}_x\tau_{\rm co} + \frac{n^{\uparrow}_x}{\tau_{\rm inco}} + \frac{n^{\uparrow}_0}{\tau^e_s} f(\Delta E_e, t) - \frac{n^{\downarrow}_0}{\tau^e_s} f(-\Delta E_e, t) - \frac{n^{\downarrow}_0}{\tau_{e0}} - \frac{n^{\downarrow}_0 p^{\downarrow}_0}{\tau_0} = 0, \tag{5}$$

$$\frac{dn^{\uparrow}_{hx}}{dt} = R - p^{\uparrow}_x\left(\frac{1}{\tau_{\rm cop}} + \frac{1}{\tau_{\rm incop}}\right) - \frac{p^{\uparrow}_x}{\tau^h_s} f\left(\Delta E^x_h, t\right) + \frac{p^{\downarrow}_x}{\tau^h_s} f\left(-\Delta E^x_h, t\right) - \frac{p^{\uparrow}_x}{\tau^{ex}} = 0, \tag{6}$$

$$\frac{dn^{\downarrow}_{hx}}{dt} = R - p^{\downarrow}_x\left(\frac{1}{\tau_{\rm cop}} + \frac{1}{\tau_{\rm incop}}\right) - \frac{p^{\downarrow}_x}{\tau^h_s} f\left(-\Delta E^x_h, t\right) + \frac{p^{\uparrow}_x}{\tau^h_s} f\left(\Delta E^x_h, t\right) - \frac{p^{\uparrow}_x}{\tau^{ex}} = 0, \tag{7}$$

$$\frac{dn^{\uparrow}_{h0}}{dt} = p^{\uparrow}_x\tau_{\rm cop} + \frac{p^{\downarrow}_x}{\tau_{\rm incop}} - \frac{p^{\uparrow}_0}{\tau^h_s} f(\Delta E_h, t) + \frac{p^{\downarrow}_0}{\tau^h_s} f(-\Delta E_h, t) - \frac{p^{\uparrow}_0}{\tau_{e0}} - \frac{n^{\uparrow}_0 p^{\uparrow}_0}{\tau_0} = 0, \tag{8}$$

$$\frac{dn_{h0}^{\downarrow}}{dt} = p_x^{\downarrow}\tau_{\text{cop}} + \frac{p_x^{\uparrow}}{\tau_{\text{incop}}} + \frac{p_0^{\uparrow}}{\tau_s^h} f(\Delta E_h, t) - \frac{p_0^{\downarrow}}{\tau_s^h} f(-\Delta E_h, t) - \frac{p_0^{\downarrow}}{\tau_{e0}} - \frac{n_0^{\downarrow} p_0^{\downarrow}}{\tau_0} = 0. \quad (9)$$

Note that we have also considered incoherent relaxation times to account for any additional relaxation or recombination effect beyond the transition between the eight levels described in Fig. 3(a). There are, *a priori*, no spin-asymmetric parameters, as presumed in Ref. [22], but the thermalization induced by the magnetic field which is tuned by the spin splitting and ruled by the Boltzmann factor [$f(x, T) = e^{-\frac{x}{kT}}$ for $x \geqslant 0$ and equals to 1, otherwise]. This model also allows exploring the asymmetry between conduction and valence band parameters that is proven to play a major role in the contrasting thermalization of electrons and holes [34]. Finally, the PL intensity is considered proportional to the terms $P^{\uparrow\downarrow} = \frac{n_0^{\uparrow\downarrow} p_0^{\uparrow\downarrow}}{\tau_0}$ and the DCP is given by $\text{DCP} = \frac{P^{\uparrow} - P^{\downarrow}}{P^{\uparrow} + P^{\downarrow}}$.

Before discussing in detail the solutions of Eqs. (2)–(9), we must state that a simple thermalization in the spin-split ground states, as described by Eqs. (4), (5), (8), and (9), could in principle produce an inversion of the DCP with temperature by just considering asymmetric Zeeman splittings and spin relaxations between the conduction and valence bands. This is fully disclosed in the Supplemental Material of this work [31]. However, no power induced DCP inversion is attained in such a simplified system. Thus, this reinforces the need of considering the excited states too that, as we already demonstrated, are contributing to the relaxation dynamics.

By assuming inverted Zeeman splitting in the conduction and valence bands, $\Delta E_{e0} = -\Delta E_{h0}$ and $\Delta E_{ex} = -\Delta E_{hx}$, the eight-level system provides a tuning of the DCP with temperature as shown in Fig. 3(b). To assess the impact of differing valence and conduction band parameters, we introduced the symmetry parameter $\alpha = \frac{\tau_s^h}{\tau_s^e}$. Note that this ratio is what enables the occurrence of a sign inversion with temperature, T. The effect can also be tuned with incident light power, as displayed in Fig. 3(c) for the same set of intrinsic parameters as in panel (a). In this case, a nonmonotonic function emerges as a function of temperature, exhibiting a peak in the DCP before collapsing to zero. In Fig. 3(d), we have plotted the DCP vs excitation power for a fixed temperature. The value of the symmetry parameter α determines whether the functional dependence with power shrinks or grows and if an eventual DCP inversion is present. The shift with temperature in this case has also been shown in Fig. 3(e).

Now, we are able to compare the model and the experimental results. To emulate the experimental results of Fig. 4(a), the best energy values were $\Delta E_e = -0.06$ meV and $\Delta E_h = 0.1$ meV. The excitation power dependence of the DCP shows a sign inversion at low temperature and there is a good convergence for 8 K. As discussed in Ref. [28], the effective temperature is expected to rise with incident power. On the other hand, the excitation power values used to fit the experimental results for DCP vs temperature, in Fig. 4(b), varied between 1 to 100 μW, where the best convergence was for 10 μW, at least for temperatures up to 40 K. For higher temperatures none of the values of excitation power could fit the experimental results. We can ascribe this to the temperature dependence of the rates of incoherent mechanisms which is a factor that the current model is neglecting by assuming all the parameters constant with temperature. As reported in Ref. [28], incoherent processes can be boosted with increasing T, further reducing the DCP.

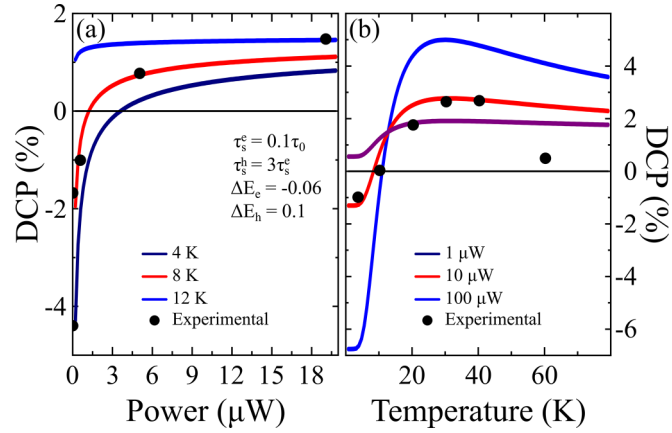

FIG. 4. Experimental (dots) and theoretical results (lines) for DCP vs (a) excitation power for different temperatures and (b) temperature for different excitation powers. Both using $\tau_s^e = 0.1\tau_0$ and $\tau_s^h = 3\tau_s^e$. The presented results are the best combination for temperature (a) and excitation power (b) with ΔE_e and ΔE_h values on an eight-level system.

The four-level model is elaborated and depicted in the Supplemental Material [31] (refer to Fig. S2 therein) to demonstrate that a simplified dynamics fails to replicate the primary experimental trends, necessitating the utilization of the eight-level system. We also underscore that strain was dismissed as a hypothesis for interpreting the disparate spin responses on the (100) and (311)A substrates, as no significant discrepancies were observed in the x-ray diffraction measurements for both samples also described in the Supplemental Material (refer to Fig. S3 and Tables S1 and S2) [31].

IV. CONCLUSION

In conclusion, our investigation delved into the spin response of GaAs/AlGaAs multiquantum wells (MQWs) grown on both (100) and (311)A GaAs substrates, comparing their optical properties under an applied external magnetic field. In both samples, we observed intensity oscillations at high magnetic fields, which were successfully described by the magnetoabsorption model. This model elucidates how the alignment between the excitation photon energy and the Landau level subbands leads to absorption maxima. This underscores the significant contribution of coherent spin relaxation from excited states in this phenomenon. Furthermore, we explored the influence of external parameters on the magneto-PL measurements. Remarkably, we discovered that the QW grown on the (311)A surface exhibited a reversal in the degree of circular polarization (indicative of spin dominance) with increasing excitation power and temperature, a phenomenon absent in the (100) substrate. To explain these experimental findings, we developed an eight-level system that incorporates not only ground state transitions but also electron and hole excited

states that were experimentally proven relevant. Our model unequivocally demonstrates that thermalization plays a pivotal role in reproducing the inversion of spin character, eliminating the necessity for arguments based on spin-dependent relaxation rates, as previously suggested in the literature. This insight sheds new light on the mechanisms governing spin dynamics in semiconductor nanostructures and underscores the importance of considering complex energy level structures in interpreting experimental observations.

ACKNOWLEDGMENTS

This study was financed in part by the Fundação de Amparo à Pesquisa do Estado de São Paulo (Grants No. 2013/18719-1, No. 2014/19142-2, No. 2017/23668-8, No. 2018/01914-0, No. 2018/06328-1, No. 2022/08731-3, and No. 2022/10340-2), CAPES and Conselho Nacional de Desenvolvimento Científico e Tecnológico (CNPq) (Grants No. 164765-2018-2 and No. 304404/2023-3).

[1] S. A. Wolf, D. D. Awschalom, R. A. Buhrman, J. M. Daughton, S. von Molnár, M. L. Roukes, A. Y. Chtchelkanova, and D. M. Treger, Science **294**, 1488 (2001).

[2] A. Hernández-Mínguez, K. Biermann, R. Hey, and P. V. Santos, Phys. Status Solidi B **251**, 1736 (2014).

[3] S. Ullah, G. M. Gusev, A. K. Bakarov, and F. G. G. Hernandez, Pramana - J. Phys. **91**, 34 (2018).

[4] G. Liu, Y. Chen, Y. Liu, C. Jia, and Z. Wang, J. Apply. Phys. **104**, 064321 (2008).

[5] A. Hernández-Mínguez, K. Biermann, R. Hey, and P. V. Santos, Phys. Rev. B **94**, 125311 (2016).

[6] G. Wang, A. Balocchi, A. V. Poshakinskiy, C. R. Zhu, S. A. Tarasenko, T. Amand, B. L. Liu, and X. Marie, New J. Phys. **16**, 045008 (2014).

[7] S. L. Chen, T. Kiba, X. J. Yang, J. Takayama, and A. Murayama, Apply. Phys. Lett. **108**, 152103 (2016).

[8] E. Margapoti, F. M. Alves, S. Mahapatra, T. Schmidt, V. Lopez-Richard, C. Destefani, E. Menéndez-Proupin, F. Qu, C. Bougerol, K. Brunner, A. Forchel, G. E. Marques, and L. Worschech, Phys. Rev. B **82**, 205318 (2010).

[9] L. K. Castelano, D. F. Cesar, V. Lopez-Richard, G. E. Marques, O. D. D. Couto, F. Iikawa, R. Hey, and P. V. Santos, Phys. Rev. B **84**, 205332 (2011).

[10] C. Aku-Leh, F. Perez, B. Jusserand, D. Richards, and G. Karczewski, Phys. E Low-Dimens. Syst. Nanostruct. **40**, 1865 (2008).

[11] K. Ploog, in *Physics, Fabrication, and Applications of Multilayered Structures*, edited by P. Dhez and C. Weisbuch (Springer, Boston, 1988), pp. 33–36.

[12] Y. Sun, T. Nishida, and S. E. Thompson, *Strain Effect in Semiconductors* (Springer, US, 2010), pp. 23–49.

[13] K. Moratis, J. Cibert, D. Ferrand, and Y.-M. Niquet, Phys. Rev. B **103**, 245304 (2021).

[14] L. Balaghi, G. Bussone, R. Grifone, R. Hübner, J. Grenzer, M. Ghorbani-Asl, A. V. Krasheninnikov, H. Schneider, M. Helm, and E. Dimakis, Nat. Commun. **10**, 2793 (2019).

[15] M. Jeannin, A. Artioli, P. Rueda-Fonseca, E. Bellet-Amalric, K. Kheng, R. André, S. Tatarenko, J. Cibert, D. Ferrand, and G. Nogues, Phys. Rev. B **95**, 035305 (2017).

[16] T. Taliercio, A. Gassenq, E. Luna, A. Trampert, and E. Tournié, Apply. Phys. Lett. **96**, 062109 (2010).

[17] S. D. Singh, S. Porwal, T. K. Sharma, and S. M. Oak, J. Apply. Phys. **112**, 093505 (2012).

[18] J. Ibáñez, R. Kudrawiec, J. Misiewicz, M. Schmidbauer, M. Henini, and M. Hopkinson, J. Apply. Phys. **100**, 093522 (2006).

[19] J. A. Steele, R. A. Lewis, M. Henini, O. M. Lemine, and A. Alkaoud, J. Apply. Phys. **114**, 193516 (2013).

[20] C. Mailhiot and D. L. Smith, Phys. Rev. B **35**, 1242 (1987).

[21] M. Houng, Y.-C. Chang, and W. I. Wang, J. Apply. Phys. **64**, 4609 (1988).

[22] Y. V. Terent'ev, M. S. Mukhin, A. A. Toropov, M. O. Nestoklon, B. Ya. Meltser, A. N. Semenov, V. A. Solov'ev, and S. V. Ivanov, Phys. Rev. B **87**, 045315 (2013).

[23] D. F. Cesar, M. D. Teodoro, H. Tsuzuki, V. Lopez-Richard, G. E. Marques, J. P. Rino, S. A. Lourenço, E. Marega, I. F. L. Dias, J. L. Duarte, P. P. González-Borrero, and G. J. Salamo, Phys. Rev. B **81**, 233301 (2010).

[24] N. Harima, J. T. Nelson, and T. Ohachi, J. Cryst. Growth **237-239**, 274 (2002).

[25] E. Ribeiro, F. Cerdeira, and A. Cantarero, Phys. Rev. B **51**, 7890 (1995).

[26] R. Nötzel, N. N. Ledentsov, L. Däweritz, M. Hohenstein, and K. Ploog, Phys. Rev. Lett. **67**, 3812 (1991).

[27] R. C. Miller, D. A. Kleinman, and A. C. Gossard, Phys. Rev. B **29**, 7085 (1984).

[28] V. Laurindo, E. D. Guarin Castro, G. M. Jacobsen, E. R. C. de Oliveira, J. F. M. Domenegueti, B. Alén, Yu. I. Mazur, G. J. Salamo, G. E. Marques, E. Marega, M. D. Teodoro, and V. Lopez-Richard, Phys. Rev. B **105**, 045414 (2022).

[29] S. Mui, K. Ramaswamy, C. J. Stanton, S. A. Crooker, and S. E. Hayes, Phys. Chem. Chem. Phys. **11**, 7031 (2009).

[30] E. L. Sesti, D. D. Wheeler, S. E. Hayes, D. Saha, G. D. Sander, and C. J. Stanton, Phys. Rev. B **90**, 125301 (2014).

[31] See Supplemental Material at http://link.aps.org/supplemental/10.1103/PhysRevB.110.035417 for additional magneto-PL data, fourth-level model, and x-ray diffraction measurements, which includes Ref. [35].

[32] L. M. Roth, B. Lax, and S. Zwerdling, Phys. Rev. **114**, 90 (1959).

[33] R. Winkler, S. J. Papadakis, E. P. De Poortere, and M. Shayegan, Spin-orbit coupling in two-dimensional electron and hole systems, in *Advances in Solid State Physics*, edited by B. Kramer (Springer Berlin, Heidelberg, Berlin, 2001), pp. 211–223.

[34] E. D. Guarin Castro, A. Pfenning, F. Hartmann, G. Knebl, M. D. Teodoro, G. E. Marques, S. Höfling, G. Bastard, and V. Lopez-Richard, J. Phys. Chem. C **125**, 14741 (2021).

[35] D. Kriegner, E. Wintersberger, and J. Stangl, J. Appl. Crystallogr. **46**, 1162 (2013).